Talanta 201 (2019) 511–518

Contents lists available at ScienceDirect

Talanta

journal homepage: www.elsevier.com/locate/talanta

Facile synthesis of highly ordered mesoporous Fe_3O_4 with ultrasensitive detection of dopamine

Yarong Huang[a,b,1], Yongzhao Zhang[a,b,1], Dandan Liu[c], Menggang Li[b], Yongsheng Yu[a,*], Weiwei Yang[b,*], Haibo Li[a]

[a] Key Laboratory of Functional Materials Physics and Chemistry of the Ministry of Education, Jilin Normal University, Changchun 130103, China
[b] MIIT Key Laboratory of Critical Materials Technology for New Energy Conversion and Storage, School of Chemistry and Chemical Engineering, Harbin Institute of Technology, Harbin, Heilongjiang 150001, China
[c] Department of Endocrinology, The Eighth Affiliated Hospital, Sun Yat-Sen university, Shenzhen 518033, China

ARTICLE INFO

Keywords:
Dopamine detection
Hard template
Mesoporous Fe_3O_4
Electrochemical biosensor

ABSTRACT

Dopamine (DA) detection is significant for the prevention of unfavorable neuronal illness. However, the detection of DA with low concentration still face tremendous challenges. In this study, highly ordered mesoporous Fe_3O_4 materials were synthesized as a biosensor by using mesoporous silica KIT-6 with different aging temperature as hard template. The ordered mesoporous Fe_3O_4 with high surface area modified glassy carbon electrode shows the high sensitivity for detecting DA. Fe_3O_4-40 mesoporous material modified electrode has the highest catalytic activity to DA with a sensitivity of 0.053 nA nM^{-1} and a detection limit of 0.8 nM (S/N = 3). The results indicating that the mesoporous Fe_3O_4 material modified electrode exhibits high sensitivity to determine DA at low levels, which can be used for DA real-time monitoring in neutral biological media.

1. Introduction

Dopamine (DA) plays a vital role in the mammalian central nervous system, whereas an abnormal concentration change of DA in biological fluids tends to increase the risk of diseases, such as, Parkinson, schizophrenia and drug addiction, which make accurate detection of DA in living cells becomes very important [1–4]. Considerable efforts were developed based on reliable methods for detection of DA [5–7]. However, the detection of DA in clinical analysis remain exist some constrains, including the low sensitivity, high detection limits and complicated preparation process, which make DA sensors difficult to give an accurate result [8,9]. Unlike other methods, electrochemical method has the advantages of rapid detection, simple operation, real-time detection and cost effectiveness [10].

A wide variety of materials such as polymer [11], metallic [12], and hybrid nanostructures [13] have been proposed for detecting DA. Recently, researches using noble metal materials exhibit high catalytic activity owe to their good conductivity. Electrodes modified with noble metal nanoparticles improve the sensitivity for DA detection [14]. However, the high cost of noble metal modified sensors hindered their practical application. Compared to noble metal, Fe_3O_4 attracted wide attention due to their unique properties, such as excellent biocompatibility, magnetic properties and structure tunable [15]. Fe_3O_4 with different structure applied in DA detection have been reported, such as nanoparticles [16,17], nanorod [18], nanoring [19] and nanoflowers [20]. However, these Fe_3O_4 nanostructures also show some drawbacks, such as the low electronical conductivity and easy agglomeration in the analysis process, leading to poor electrochemical performance [21]. Particularly, ordered mesoporous nanomaterials have their architectural advantages of large specific surface area, interconnected pores, regular texture, and thus provide numerous of active sites which facilitate the mass transport and electron transfer [22–25]. Furthermore, Fe_3O_4 with ordered mesoporous structure could effectively avoid the agglomeration.

Herein, we constructed an ultrahigh sensitive ordered mesoporous Fe_3O_4-based biosensor for detecting DA through a facile nanocasting method. The ordered mesoporous Fe_3O_4 with large surface area shows ultrahigh sensitivity and perfect selectivity for detection of DA with low detection limits and wide concentration ranges. As-prepared mesoporous Fe_3O_4-based biosensor is successfully for detecting DA released from living PC12 cells. The results show that ordered mesoporous Fe_3O_4-based biosensor can apply as the probe which can offer a real-time quantitative detection of DA during a neurological environment.

* Corresponding authors.
E-mail addresses: ysyu@hit.edu.cn (Y. Yu), yangww@hit.edu.cn (W. Yang).
[1] These authors contributed equally.

https://doi.org/10.1016/j.talanta.2019.01.099
Received 14 November 2018; Received in revised form 24 January 2019; Accepted 29 January 2019
Available online 30 January 2019
0039-9140/

2. Experiment section

2.1. Reagents

P123 (Triblock copolymer Pluronic, M_w = 5800,) was purchased from sigma-Aldrich. Hydrochloric acid (HCl), buty alcohol, Tetrathylorthosilicate (TEOS), ethanol, ferric nitrate ($Fe(NO_3)_3{\cdot}9H_2O$) and sodium hydroxide (NaOH) for prepared mesoporous Fe_3O_4 were purchased from Aladdin.

2.2. Apparatus

Transmission electron microscopy (TEM) was used for characterizing the mesoporous structure on a JEOL JEM-1400. The X-ray diffraction (XRD) patterns were recorded on PANanalytical X'Pert powder using Cu Kα radiation (λ = 1.5418 Å). The surface areas and pore volume of the materials were characterized by a Beishide 3H-2000PS1 Gas Sorption and Porosimetry system.

2.3. Preparation of SiO_2 template and mesoporous Fe_3O_4

Ordered mesoporous KIT-6 was prepared as follows: 3 g P123 was dissolved in 108 mL deionized water until form a homogeneous solution. 5 mL HCl was added and stirred vigorously until P123 was completely dissolved. Then adding 3 g n-butanol to the solution and placed it in a 35 °C oil bath. After 1 h stirring, 6.45 g TEOS was added into the solution. The mixture is stirred for 24 h at 35 °C. Hydrothermal treatment (40, 80, 120 °C) was applied for 24 h. After hydrothermal process, the product was precipitated and collected using filtration. The solid product was put into a crucible for calcination. The calcination temperature is 550 °C and held for 6 h. KIT-6 aged at different temperature were denoted as KIT-40, KIT-80 and KIT-120.

1 g of KIT-6 aged at 40 °C impregnated in ~0.8 M precursor solution, vigorous stirring was applied to make sure the composite can be well mixed. After the solvent completely evaporated, the vessel was placed on a hitting plate at 50 °C overnight. The dried powder was transferred into a crucible for calcination. The powder was sintered at 500 °C in the air for 5 h (heating rate: 1 °C/min). After calcination process, the powder was transferred into 2 M NaOH solution to leach the SiO_2 template. The product was washed with distilled water and collected by centrifugation for several times. Finally, the ordered mesoporous α-Fe_2O_3 was obtained by dried the products at 60 °C. Mesoporous Fe_3O_4 was achieved by annealing α-Fe_2O_3 under a 5% H_2-95% Ar atmosphere at 450 °C for 1 h. Finally, ordered mesoporous Fe_3O_4-40, Fe_3O_4-80 and Fe_3O_4-120 were fabricated from KIT-40, KIT-80 and KIT-120 [26]. The process for preparation of ordered mesoporous Fe_3O_4 was illustrate in Scheme 1.

2.4. Fabrication of electrode and electrochemical measurements

The 2 mg/mL as-prepared materials mixed with 2 mg/mL Ketjen carbon and sonicated for 30 min. The mixture was washed by ethanol three times. The products were dried under N_2 and redispersed in 3.2 mL deionized water, 0.8 mL isopropanol and 20 μL 5% Nafion, the concentration of mixture was 0.4 mg/mL. After sonicating the mixture at least 30 min, a 3 mm diameter clean glassy carbon electrode (surface area: 0.07 cm^2) was modified with 10 μL mixture solution and dried under ambient conditions. Electrochemical experiments were performed on a CHI660C workstation under a three-electrode system. Modified GCE, Ag/AgCl (in saturated KCl), and a platinum wire were used as the working, reference, and counter electrodes, respectively. The modified GCE were activated in 0.1 M PBS solution (pH 7.0) by cyclic voltammetry scanning. Cyclic Voltammetry (CV) was employed in a PBS solution with 0.1 mM DA at a scan rate of 100 mV s^{-1}. Quantitative detection of the DA with different concentrations which pulse width is 10 ms and the amplitude is 50 mV was performed by differential pulse voltammetry (DPV). Amperometric current time (*i-t*) curve was investigated in a stirred PBS solution with 0.23 V.

2.5. Measuring the flux of DA released from PC12 cells

PC12 cells were achieved from the Harbin Medical University. The cells were washed with PBS solutions and then redispersed in 2 mL PBS. Amperometric current time curves of the Fe_3O_4-40 electrodes were investigated in cell dispersion solution. After activation, adding 105 μL of KCl (2 M) solution to the cell dispersion. While stimulating with K^+, an obvious current response appears and quickly decrease to the background. Same concentration of KCl were added to stimulate the cells after PC12 cells were treated with 50 μM nifedipine solution for 30 min, but a weak current response will be obtained. The control experiment which the detection solution stimulated by KCl without cells was also carried out, no response was observed.

3. Results and discussion

3.1. Characterization of mesoporous materials

Highly ordered mesoporous Fe_3O_4 was prepared by nanocasting from a silica KIT-6 hard template, accompanying by a reduction process with H_2 (Scheme 1). The hard template KIT-6 with interconnected two mesoporous channel systems was firstly characterized by TEM. As shown in Fig. 1(a), (b) and (c), the KIT-6 silica templates prepared by different aging temperature are the highly ordered mesoporous structure, which affect the structure of nanocast metal oxides replica [27]. After nanocasting process, the well-ordered mesoporous Fe_3O_4 structures are clearly seen in Fig. 1(d), (e) and (f), which demonstrate that mesoporous Fe_3O_4 materials are replicated from KIT-6 template successfully after removal of KIT-6 template. The slit-like pores are well distributed in the entire mesoporous Fe_3O_4.

Crystalline structure of mesoporous Fe_3O_4 was characterized by X-ray diffraction (XRD) measurements. The diffraction peaks at 2θ = 30.09, 35.42, 43.05, 53.39, 56.94, 62.51 and 73.94 (Fig. 2(a)) can be indexed to the (220), (311), (400), (422), (511), (440) and (533) planes of cubic Fe_3O_4 (JPCDS Card No. 19-0629). The broad peak of mesoporous Fe_3O_4 possibly derived from the pore walls which composed by small particles [28]. No other impurity was observed. These

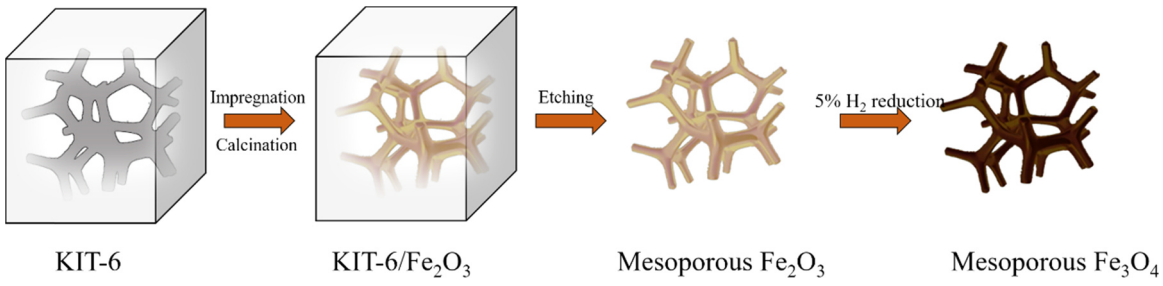

Scheme 1. Schematic illustration of the preparation process of Fe_3O_4.

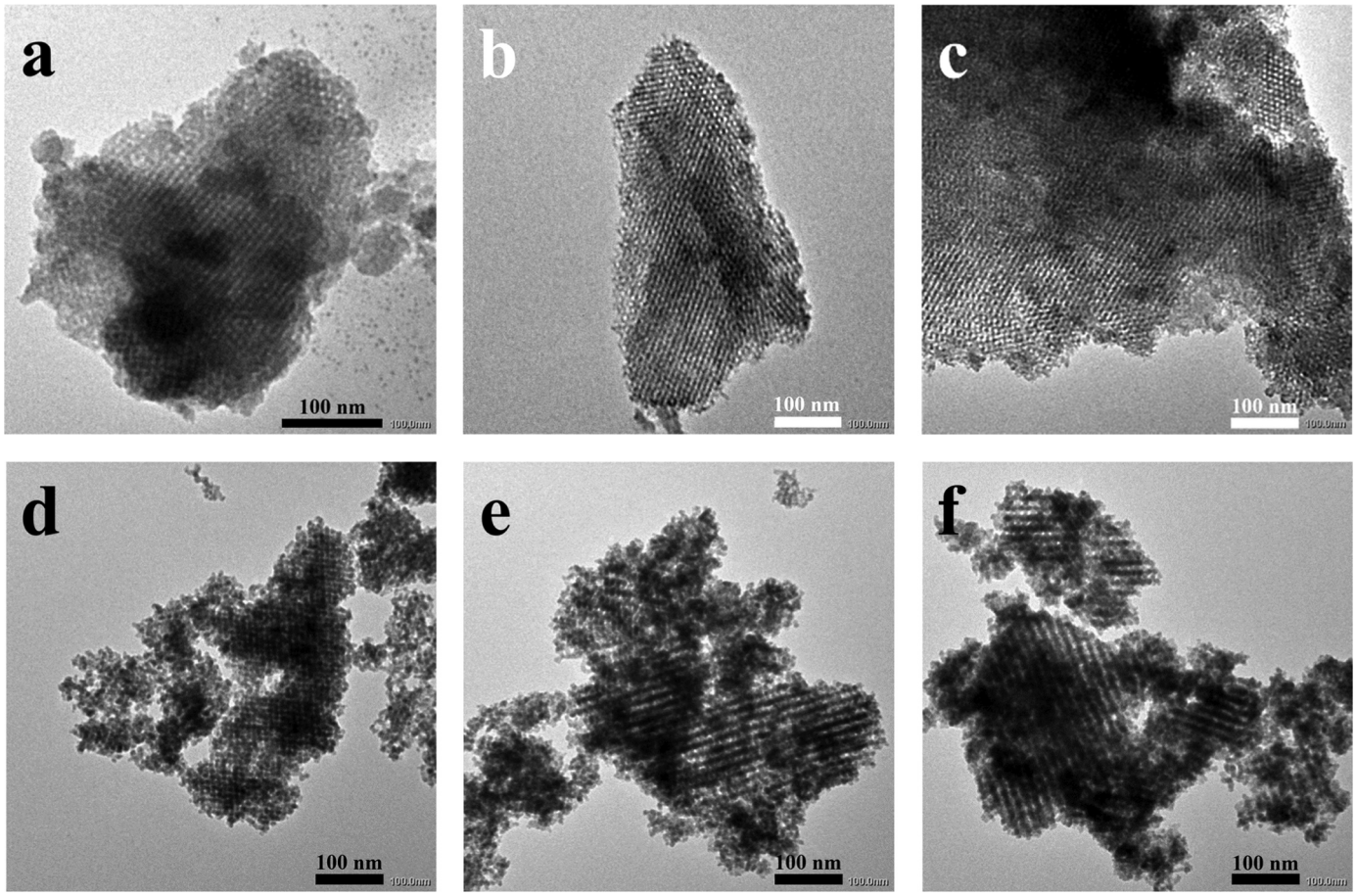

Fig. 1. TEM images of as-prepared mesoporous materials: (a) KIT-40, (b) KIT-80, (c) KIT-120, (d) Fe_3O_4-40, (e) Fe_3O_4-80 and (f) Fe_3O_4-120.

results suggest that after the reduction process, the mesoporous Fe_3O_4 materials were successfully obtained [29]. In order to confirm the existence of each element, Fe_3O_4-40 was characterized by XPS. XPS survey spectrum of Fe_3O_4-40 in Fig. 2(b) show the coexistence of C, O and Fe. As shown in Fe 2p (Fig. 2(c)), 710.5 eV and 724.3 eV are related to the oxide state binding energy of Fe $2p_{3/2}$ and Fe $2p_{1/2}$ of Fe_3O_4 [30–32].

Texture parameters of mesoporous SiO_2 and Fe_3O_4 were investigated by nitrogen physisorption. The nitrogen adsorption-desorption isotherms for mesoporous SiO_2 with different aging temperature are given in Fig. 3. The isotherms obtained from KIT-6 (Fig. 3(a)) with different aging temperature exhibit type IV features with H1 hysteresis loops according to the IUPAC classification, signifying the uniform mesoporous structure. According to the calculated Brunauer-Emmett-Teller (BET) surface area data were summarized in Table 1, KIT-40, KIT-80 and KIT-120 have the similar surface areas of 660, 980 and 900 $m^2\ g^{-1}$, respectively. The physicochemical parameters of KIT-6 are influenced by aging temperature. It is reported that the wall thicknesses of silica templates are reflected in the pore sizes of nanocast samples. The large pore size of KIT-6-120 has the thinner wall thicknesses, so that the smaller pore size will the nanocasted Fe_3O_4-120 exhibits [33]. As can be seen from Table 1, the surface area, pore volume and pore size of Fe_3O_4 increased, when decreasing the aging temperature of template. Fe_3O_4-40 shows higher surface area of 136 $m^2\ g^{-1}$, larger pore volume of 0.42 $m^2\ g^{-1}$ and pore size of 12.2 nm than Fe_3O_4-80 and Fe_3O_4-120. It is expected that the high surface area and large pore volume of the mesostructure can facilitate the transport of DA and shorten the transport path of electron, which can significantly enhance the detection ability of DA [34].

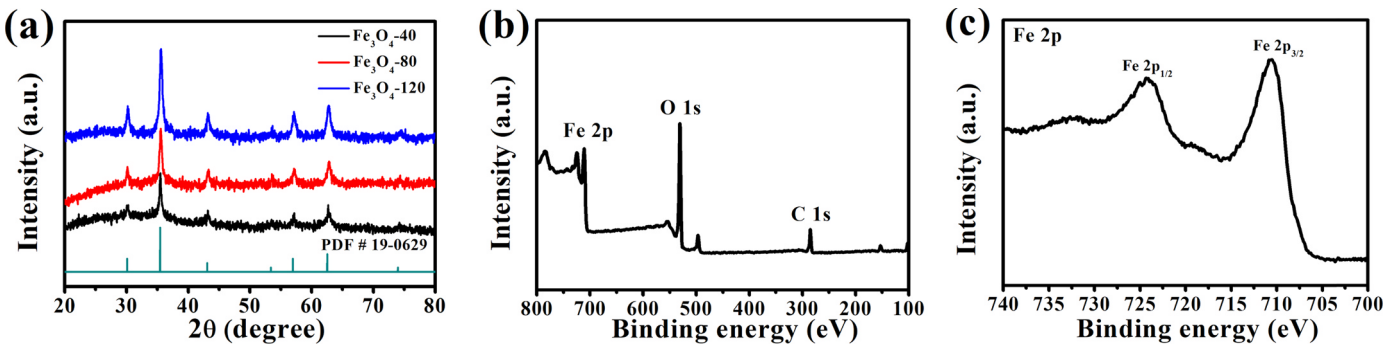

Fig. 2. (a) XRD patterns of ordered mesoporous Fe_3O_4, XPS spectra of Fe_3O_4-40: (b) broad scan spectrum, and (c) Fe 2p.

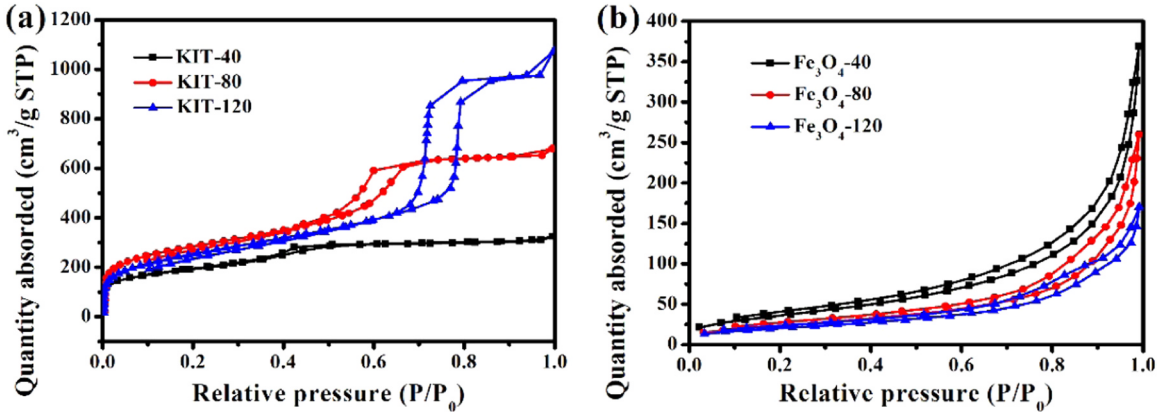

Fig. 3. Nitrogen adsorption-desorption isotherms of as-prepared materials.

Table 1
Nitrogen adsorption desorption isotherm results of as-prepared materials.

Sample	Surface area ($m^2\ g^{-1}$)	Pore volume ($cm^3\ g^{-1}$)	Pore size (nm)
KIT-40	660	0.5	3.1
KIT-80	980	1.05	5.4
KIT-120	900	1.67	9.8
Fe_3O_4-40	136	0.42	12.2
Fe_3O_4-80	90	0.31	9.1
Fe_3O_4-120	76	0.26	7.1

3.2. Electrochemical biosensor for detection of DA

Electrochemical properties of mesoporous Fe_3O_4 electrode modified GCE were characterized by CV. Fig. 4(a) shows the CV curves of Fe_3O_4-40-GCE, Fe_3O_4-80-GCE, Fe_3O_4-120-GCE, and bare GCE in a 0.1 mM PBS solution. Compare to the bare GCE electrode, a pair of well-defined redox peaks was observed in CV curves of Fe_3O_4-40-GCE, Fe_3O_4-80-GCE and Fe_3O_4-120-GCE. In addition, Fe_3O_4-40 modified GCE shows a higher peak current than Fe_3O_4-80-GCE and Fe_3O_4-120-GCE, indicating that Fe_3O_4-40 has the higher ability in the DA electrochemical

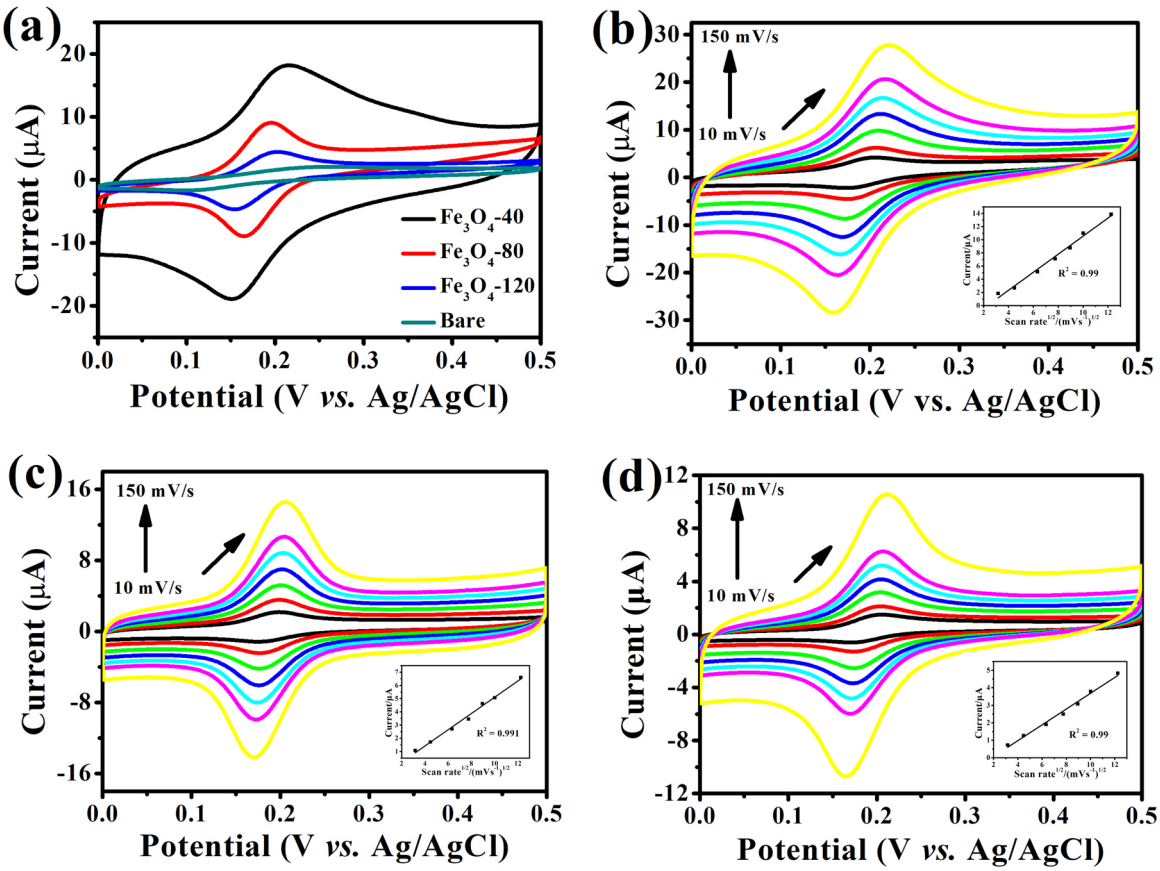

Fig. 4. (a) CV curves of PBS (pH 7.0) with 0.1 mM DA on a bare GCE, Fe_3O_4-40-GCE, Fe_3O_4-80-GCE and Fe_3O_4-120-GCE respectively, scan rate: 100 mV s^{-1}. (b)-(d) CV curves of Fe_3O_4-40-GCE, Fe_3O_4-80-GCE and Fe_3O_4-120-GCE at various rates from 10, 20, 40, 60, 80, 100, 150 mV s^{-1}, respectively. (Inset: Plot of peak current *vs.* square root of scan rates.).

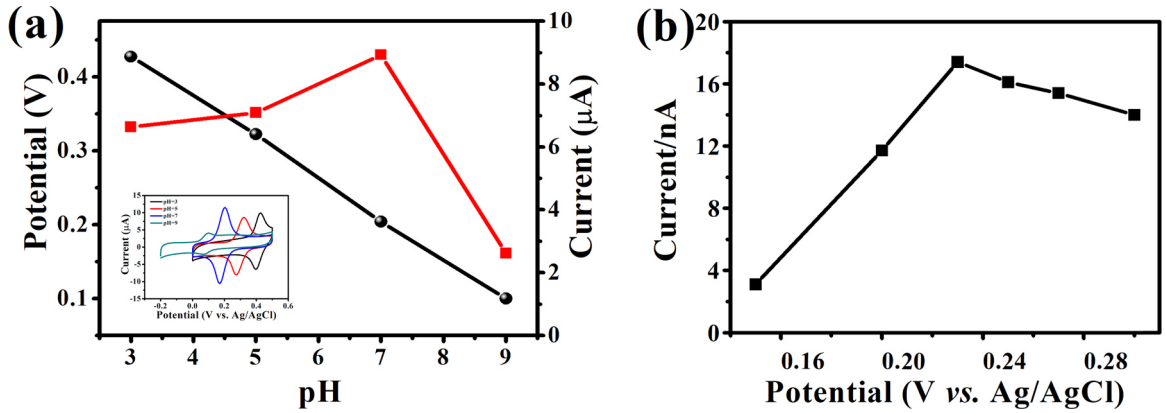

Fig. 5. (a) The plots of E_{pa} (black) and I_{pa}(red) with different pH values, Inset: CV curves of PBS for 0.1 mM DA on Fe_3O_4-40-GCE with different pH (pH = 3, 5, 7, 9, scan rate: 50 mV s^{-1}), (b) Current-time curves of Fe_3O_4-40-GCE in PBS with different potential. (b) Current-time curves of Fe_3O_4-40-GCE in PBS with different potential.

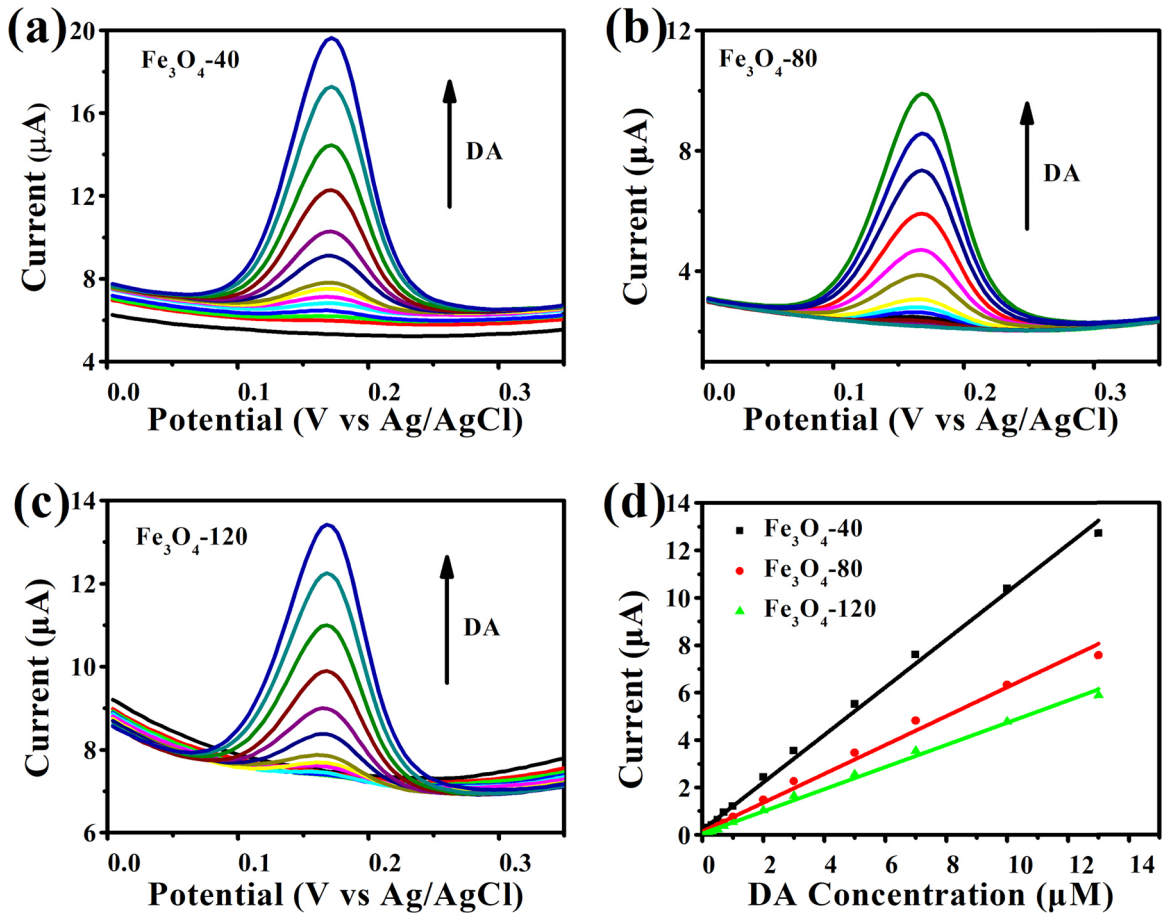

Fig. 6. DPV curves of DA from 0 μM to13 μM at (a) Fe_3O_4-40-GCE, (b) Fe_3O_4-80-GCE, (c) Fe_3O_4-120-GCE (0.1 M PBS solution). (d) Plots of the I_{pa} against with various concentration of DA for the Fe_3O_4-40-GCE, Fe_3O_4-80-GCE, Fe_3O_4-120-GCE.

oxidation. Mesoporous structure with high surface area can make ion and electron transport efficiently. Fig. 4(b)-(d) shows the CV curves of Fe_3O_4-40-GCE, Fe_3O_4-80-GCE and Fe_3O_4-120-GCE under different scan rates. The oxidative peak currents increased linearly with the square root of scan rate with a square of regression coefficient (R^2) of 0.99, 0.991 and 0.99 (Inset of Fig. 4(b)-(d)), which indicate that the electro-redox of DA on the Fe_3O_4-GCE was a typical diffusion-controlled process. Salamon et al. have reported the mechanism of dopamine detection on the Fe_3O_4-modified electrode, Fe^{3+} originated from Fe_3O_4 can make DA oxidized into dopamine-o-quinone, and the Fe^{3+} and Fe^{2+} can transformed and regenerated through the reaction process [18].

The influence of pH in detection of DA is shown in new Fig. 5(a). The influence of pH on the Fe_3O_4-40 modified electrode was studied by cyclic voltammetry. In Fig. 5(a), Fe_3O_4-40 modified electrode was employed in a PBS solution (pH = 3, 5, 7, 9) with 0.1 mM DA at a scan rate of 50 mV s^{-1}. The slope value of −54.9 mV/pH (y = −0.0549 + 0.5929x, R^2 = 0.9991) is close to the reported theoretical slope value (−59 mV/pH), which confirms that the electrochemical redox process of DA is a two electrons and two protons process. Before amperometric current-time measurement, we also tested

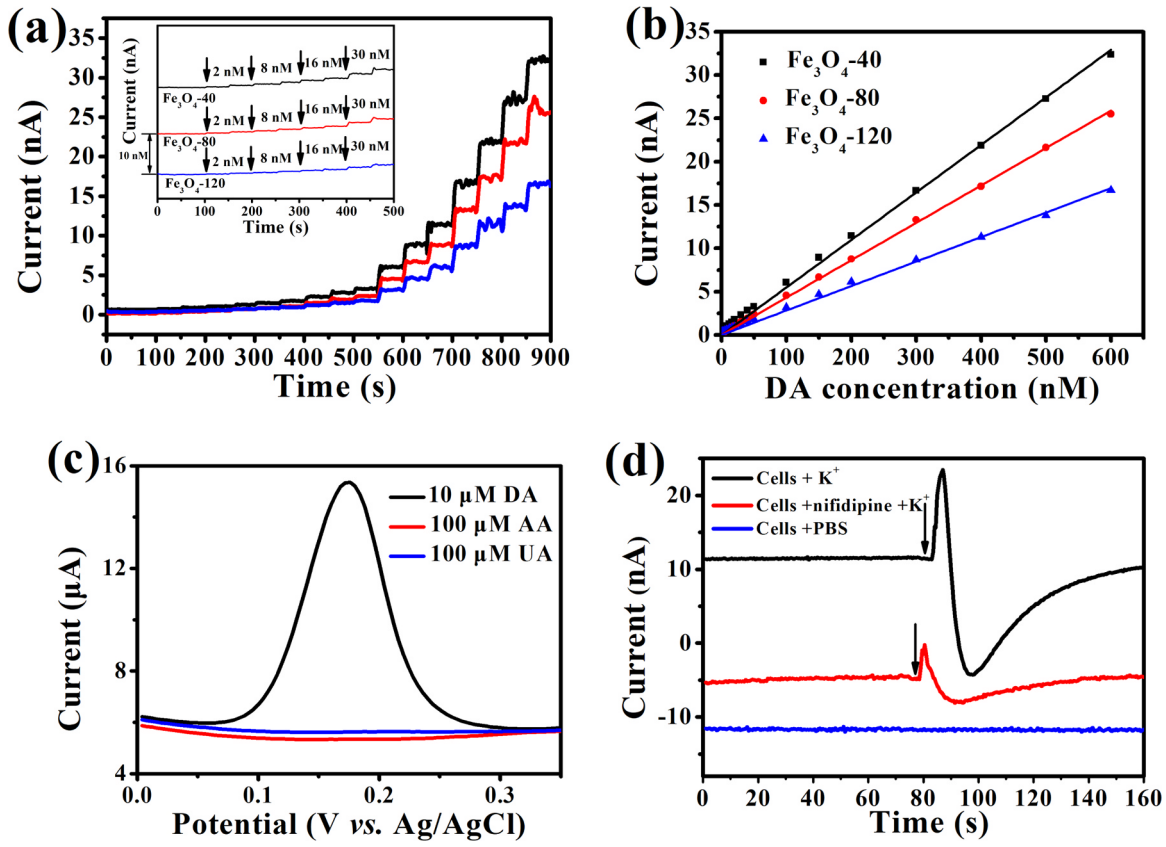

Fig. 7. (a) Current-time curves of the mesoporous Fe_3O_4 materials modified electrodes on the addition of DA in PBS, the potential is 0.23 V *vs.* Ag/AgCl. (Inset: The partial enlargement from 0 s to 500 s) (b) The plot of mesoporous Fe_3O_4 materials-modified electrodes between the current response and DA concentration. (c) DPV responses of Fe_3O_4-40-GCE interfered with 100 μM various species (UA, AA) and 10 μM of DA, 0.1 M PBS. (d) An obvious *i-t* response recorded for released dopamine from living PC12 cells at Fe_3O_4-40-GCE upon stimulated by 100 mM KCl (black). After being treated with nifedipine (50 μM) for 30 min, same concentration of K^+ solutions were added to stimulate the cells (red). PC12 cells dispersed in PBS solution without K^+ stimulation upon Fe_3O_4-40-GCE (blue). The arrow shows the time when adding high K^+ buffer into the PBS.

the effect of different potential for Fe_3O_4-40 modified electrode, the result is shown in the Fig. 5(b). When the potential is 0.23, the current values in i-t curves is largest.

Differential pulse voltammetry (DPV), which has the advantages of improving sensitivity and better analytical applications characteristics, was used to detect different concentration additions of DA (Fig. 6). A series of anode current responses were obtained at about 0.17 V in the presence of DA, which was attributed to the DA oxidation. The anodic peak current (I_{pa}) increases with the DA concentration in the range from 0.04 μM to 13 μM for each electrode (Fig. 6(a)-(c)), which exhibits an excellent linear relationship with the DA concentration (Fig. 6(d)). The linear regression equation was used to calculate the sensitivity of DPV, Fe_3O_4-40 exhibit a much higher sensitivity of 1.003 μA μM^{-1} (I_{pa} (μA) = 1.003c (μM) + 0.206 (R^2 = 0.996)) than either the Fe_3O_4-80 (I_{pa} (μA) = 0.609c (μM) + 0.138 (R^2 = 0.991)) or the Fe_3O_4-120 (I_{pa} (μA) = 0.468 c (μM) + 0.053 (R^2 = 0.996)).

Amperometric current-time technique (*i-t*) was used for detecting low concentration of DA in 0.1 M PBS (the potential: 0.23 V *vs.* Ag/AgCl). In Fig. 7(a), a well-defined, stable and steeply increased amperometric current response was obtained after each addition of DA solution, response time is within 5 s, the calibration plot was linearly proportional to the concentration of dopamine increased ranging from 2 nM to 600 nM (Fig. 7(b)). An obvious response signal can be detected even when 2 nM DA solution was added. This rapid oxidation response can be attributed to the mesoporous structure. In the mesoporous Fe_3O_4, not only DA can rapidly absorb and transport on the surface or pore of Fe_3O_4, but also the electron can transfer rapidly. This unique structure improved the electrocatalytic activity of mesoporous Fe_3O_4 toward DA oxidation. The detection sensitivity of modified electrode calculated through the linear regression equation, the Fe_3O_4-40-GCE exhibit a sensitivity of 0.053 nA nM^{-1}, which is much higher than either the Fe_3O_4-80-GCE (0.043 nA nM^{-1}) or the Fe_3O_4-120-GCE (0.027 nA nM^{-1}). Moreover, based on signal-to-noise ratio (S/N) of 3, the detection limit of Fe_3O_4-40-GCE was estimated to be 0.8 nM, which is more sensitive than the Fe_3O_4-80-GCE (1.6 nM) and Fe_3O_4-120-GCE (2.2 nM). In fact, the excellent electrocatalytic activity of the Fe_3O_4-40-GCE can be attributed to the higher surface area and larger pore volume, which indicates that mesoporous Fe_3O_4 can enable fast adsorption and activation of DA molecules and has capable of detecting DA with extremely low concentration. The detection limit of the Fe_3O_4 for DA detection is superior to most of other reported DA sensors (Table 2). The selectivity is another key factor to determine the practical application of electrochemical sensors. Among organisms containing DA, uric acid (UA) and ascorbic acid (AA) usually coexist and have an oxidation potential similar to DA, which will make a confusion among selectively detect DA. In this work, the effects on the DA response of UA and AA were investigated. Fig. 7(c) shows the typical differential pulse voltammetry responses upon addition of 10 μM DA, 100 μM UA and AA into 0.1 M PBS. It is found that only DA exhibit an obvious anodic current response while other interferences have not been observed any well-defined signals even if their concentration reach ten times of DA. This result suggested that the as-prepared mesoporous Fe_3O_4-based sensor exhibited an excellent selectivity towards DA. In order to evaluate the reproducibility of Fe_3O_4-40-GCE, CV was employed for test. The reproducibility of 4 different Fe_3O_4-40-GCE are found with an RSD (relative standard deviation) of 2.6% for detection of 0.1 mM DA. There

Table 2
Comparison of mesoporous Fe_3O_4 dopamine sensors with other electrochemical sensors used for detection of dopamine.

Electrode material	Method	Dynamic range(μM)	Detection potential window in CV (V)	Detection potential in CV (V)	Detection limit (nM)	Ref
Fe_3O_4-40	Amperometry	0.002–0.6	0–0.5	0.223	0.8	This work
PANI-Fe_3O_4	DPV	0.2–2.4	−0.2–0.8	0.2	17.6	[7]
H-Fe_3O_4@C/GNS	DPV	0.1–150	−0.2–0.6	0.14	53	[17]
rGO/Fe_3O_4	Amperometry	0.01–100.55	−0.2–0.6	0.25	7	[18]
Fe_3O_4 NRs	DPV	0.01–1	−0.2–0.8	~0.3	10	[19]
Fe_3O_4/rGO/GCE	Amperometry	0.01–0.27	−0.2–0.6	0.3	5	[20]
GO/Fe_3O_4@SiO_2 nanocomposite	DPV	0.1-600	−0.2–0.6	0.21	89	[40]
dumbbell-like FePt-Fe_3O_4	Amperometry	0.005–0.11	0–0.5	~0.23	1	[41]
doped-PPy/Fe_3O_4/rGO	DPV	0.007–1.2	−0.2–0.8	0.4	2.33	[42]
Silica-coated nanoparticles of Fe_3O_4	DPV	1–30.6	−0.2–1	—	12	[43]

were no obvious changes detected from CV curves after comparing the 10 days stability test. Finally, we investigated the potential application of Fe_3O_4-40-GCE electrode by analyzing the released DA from living PC12 cells. Amperometric current-time trace recorded during potassium-induced DA exocytosis from a population of PC12 cells. In Fig. 7(d) (black), a well-defined current response was observed after adding 100 mM KCl, the response originated from DA oxidation, which confirms that the traced amounts of released DA from a living cell can be determined rapidly by Fe_3O_4-40. The number of dopamine released from PC 12 cells can be calculated by using amperometric current time (*i-t*) curve. It is reported that the numbers of released DA calculated according the equation: $N = Q/nQ_e$, where N is number of moles of DA, Q is obtained from the integration of amperometric spikes from the DA release in a PC12 cell (9.235×10^{-8} C), n is the two electrons that donated by DA and Q_e is the charge of a single electron (1.602×10^{-19} C) [35–37]. The number of detected DA is about 2.88×10^{11}. The K^+ stimulation which can be defined as a trigger that make cells exocytosis and release DA in the PC12 cells causes depolarization of the cell membrane and induces an influx of Ca^{2+} through opening of voltage-sensitive Ca^{2+} channels [38]. To determine whether the observed response was attributed to the stimulation to proposed sensor by K^+, PBS solution only contain the PC12 cells solution sample without K^+ stimulation was prepared to perform control experiments (Fig. 7(d), blue), no current response was observed in the experiments. This indicated that nifidipine have the ability to inhibit the K^+ stimulation [39]. Therefore, we treated the PC12 cells with 50 μM nifidipine for 30 min, and then added 100 mM KCl for stimulation, a weak current response was observed (Fig. 7(d), red). Collectively, mesoporous Fe_3O_4 have the potential to be an efficient sensor for detecting DA in biological solution.

4. Conclusions

In summary, highly ordered mesoporous Fe_3O_4 materials have been prepared successfully by a facile hard template nanocasting method. The effects of mesoporous Fe_3O_4 with high surface area and large pore volume on detecting DA were systematically researched. Mesoporous Fe_3O_4-40-GCE with highest surface area and largest pore volume displays a lowest detection limit of 0.8 nM (S/N = 3) with a linear range between 2 nM and 600 nM. The fabricated mesoporous Fe_3O_4-40-GCE sensor can be applied in the real-time detection of released DA from living PC12 cells. This work suggests that ordered mesoporous Fe_3O_4 materials are a new type of high-efficiency biosensor for selective, sensitive and rapid determine of DA.

Acknowledgements

This work was supported by the National Natural Science Foundation of China under Grant (No. 51571072), Fundamental Research Funds for the Central Universities (No. AUGA5710012715), Heilongjiang Postdoctoral Scientific Research Development Fund (No. LBH-Q14058), China Postdoctoral Science Foundation (No. 2015M81436) and Heilongjiang Postdoctoral Science Foundation (No. LBH-Z15065).

References

[1] Q.L. Yuan, Y. Liu, C. Ye, H.Y. Sun, D. Dai, Q.P. Wei, G.S. Lai, T.Z. Wu, A.M. Yu, L. Fu, K.W.A. Chee, C.T. Lin, Highly stable and regenerative graphene-diamond hybrid electrochemical biosensor for fouling target dopamine detection, Biosens. Bioelectron. 111 (2018) 117–123.
[2] H.L. Ye, H. Wang, B.H. Zhang, F.Q. Zhao, B.Z. Zeng, Tremella-like $ZnIn_2S_4$/graphene composite based photoelectrochemical sensor for sensitive detection of dopamine, Talanta 186 (2018) 459–466.
[3] Y.S. He, C.G. Pan, H.X. Cao, M.Z. Yue, G.X. Liang, Highly sensitive and selective dual-emission ratiometric fluorescence detection of dopamine based on carbon dots-gold nanoclusters hybrid, Sens. Actuators B-Chem. 265 (2018) 371–377.
[4] X.Y. Chen, Q.Q. Liu, M.H. Liu, X.Y. Zhang, S.Y. Lin, Y.S. Chen, J.Y. Zhuang, D.P. Yang, Protein-templated Fe_2O_3 microspheres for highly sensitive amperometric detection of dopamine, Microchim. Acta 185 (2018) 340–347.
[5] W.J. Hu, Y.Y. Huang, C.Y. Chen, Y.K. Liu, T. Guo, B.O. Guan, Highly sensitive detection of dopamine using a graphene functionalized plasmonic fiber-optic sensor with aptamer conformational amplification, Sens. Actuators B-Chem. 264 (2018) 440–447.
[6] Y.M. Leng, K. Xie, L.Q. Ye, G.Q. Li, Z.W. Lu, J.B. He, Gold-nanoparticle-based colorimetric array for detection of dopamine in urine and serum, Talanta 139 (2015) 89–95.
[7] O.E. Fayemi, A.S. Adekunle, B.E.K. Swamy, E.E. Ebenso, Electrochemical sensor for the detection of dopamine in real samples using polyaniline/NiO, ZnO, and Fe_3O_4 nanocomposites on glassy carbon electrode, J. Electroanal. Chem. 818 (2018) 236–249.
[8] Y.L. Sun, Y.N. Lin, C.F. Ding, W.Y. Sun, Y.X. Dai, X.D. Zhu, H. Liu, C.N. Luo, An ultrasensitive and ultraselective chemiluminescence aptasensor for dopamine detection based on aptamers modified magnetic mesoporous silica@graphite oxide polymers, Sens. Actuators B-Chem. 257 (2018) 312–323.
[9] C. Sumathi, C.V. Raju, P. Muthukumaran, J. Wilson, G. Ravi, Au-Pd bimetallic nanoparticles anchored on α-Fe_2O_3 nonenzymatic hybrid nanoelectrocatalyst for simultaneous electrochemical detection of dopamine and uric acid in the presence of ascorbic acid, J. Mater. Chem. B 4 (2016) 2561–2569.
[10] G. Gao, Z.K. Zhang, K. Wang, Q. Yuan, X. Wang, One-pot synthesis of dendritic Pt_3Ni nanoalloys as nonenzymatic electrochemical biosensors with high sensitivity and selectivity for dopamine detection, Nanoscale 9 (2017) 10998–11003.
[11] G.X. Wang, A. Morrin, M.R. Li, N.Z. Liu, X.L. Luo, Nanomaterial-doped conducting polymers for electrochemical sensors and biosensors, J. Mater. Chem. B 6 (2018) 4173–4190.
[12] M.S. Hsu, Y.L. Chen, C.Y. Lee, H.T. Chiu, Gold nanostructures on flexible substrates as electrochemical dopamine sensors, ACS Appl. Mater. Interfaces 4 (2012) 5570–5575.
[13] S. Chandra, H. Lang, D. Bahadur, Polyaniline-iron oxide nanohybrid film as multifunctional label-free electrochemical and biomagnetic sensor for catechol, Anal. Chim. Acta 795 (2013) 8–14.
[14] R.Y. Li, T.T. Yang, Z.J. Li, Z.G. Gu, G.L. Wang, J.K. Liu, Synthesis of palladium@gold nanoalloys/nitrogen and sulphur-functionalized multiple graphene aerogel for electrochemical detection of dopamine, Anal. Chim. Acta 954 (2017) 43–51.
[15] B. Hu, Y.K. Liu, Z.W. Wang, Y.P. Song, M.H. Wang, Z.H. Zhang, C.S. Liu, Bimetallic-organic framework derived porous Co_3O_4/Fe_3O_4/C-loaded g-C_3N_4 nanocomposites as nonenzymic electrocatalysis oxidization toward ascorbic acid, dopamine acid, and uric acid, Appl. Surf. Sci. 441 (2018) 694–707.
[16] S. Mumtaz, L.S. Wang, S.Z. Hussain, M. Abdullah, Z. Huma, Z. Iqbal, B. Creran, V.M. Rotello, I. Hussain, Dopamine coated Fe_3O_4 nanoparticles as enzyme mimics for the sensitive detection of bacteria, Chem. Commun. 53 (2017) 12306–12308.
[17] H. Song, G.P. Xue, J.J. Zhang, G. Wang, B.C. Ye, S.G. Sun, L.P. Tian, Y.C. Li, Simultaneous voltammetric determination of dopamine and uric acid using carbon-encapsulated hollow Fe_3O_4 nanoparticles anchored to an electrode modified with nanosheets of reduced graphene oxide, Microchim. Acta 184 (2017) 843–853.

[18] J. Salamon, Y. Sathishkumar, K. Ramchandran, Y.S. Lee, D.J. Yoo, A.R. Kim, G.G. Kumar, One-pot synthesis of magnetite nanorods/graphene composites and its catalytic activity toward electrochemical detection of dopamine, Biosens. Bioelectron. 64 (2015) 269–276.
[19] X.N. Liu, F.H. Zhu, W. Wang, J.H. Lei, G.F. Yin, Synthesis of single-crystalline iron oxide magnetic nanorings as electrochemical biosensor for dopamine detection, Int. J. Electrochem. Sci. 11 (2016) 9696–9703.
[20] G.J. Rani, K.J. Babu, G.G. Kumar, M.A.J. Rajan, Watsonia meriana flower like Fe_3O_4/reduced graphene oxide nanocomposite for the highly sensitive and selective electrochemical sensing of dopamine, J. Alloy. Compd. 688 (2016) 500–512.
[21] Z.K. Li, Y.J. Zheng, T.T. Gao, Z.H. Liu, J. Zhang, G.W. Zhou, Fabrication of biosensor based on core-shell and large void structured magnetic mesoporous microspheres immobilized with laccase for dopamine detection, J. Mater. Sci. 53 (2018) 7996–8008.
[22] C.L. Xiao, X.Y. Zhang, T. Mendes, G.P. Knowles, A. Chaffee, Highly ordered hierarchical mesoporous $MnCo_2O_4$ with cubic *Iα3d* symmetry for electrochemical energy storage, J. Phys. Chem. C 120 (2016) 23976–23983.
[23] X.H. Deng, K. Chen, H. Tüysüz, Protocol for the nanocasting method: preparation of ordered mesoporous metal oxides, Chem. Mater. 29 (2017) 40–52.
[24] T.T. Sun, L.B. Xu, Y.S. Yan, A.A. Zakhidov, R.H. Baughman, J.F. Chen, Ordered mesoporous nickel sphere arrays for highly efficient electrocatalytic water oxidation, ACS Catal. 6 (2016) 1446–1450.
[25] Y.J. Sa, K. Kwon, J.Y. Cheon, F. Kleitz, S.H. Joo, Ordered mesoporous Co_3O_4 spinels as stable, bifunctional, noble metal-free oxygen electrocatalysts, J. Mater. Chem. A 1 (2013) 9992–10001.
[26] F. Jiao, J.C. Jumas, M. Womes, A.K. Chadwick, A. Harrison, P.G. Bruce, Synthesis of ordered mesoporous Fe_3O_4 and γ-Fe_2O_3 with crystalline walls using post-template reduction/oxidation, J. Am. Chem. Soc. 128 (2006) 12905–12909.
[27] Y.Y. Sun, G.B. Ji, M.B. Zheng, X.F. Chang, S.D. Li, Y. Zhang, Synthesis and magnetic properties of crystalline mesoporous $CoFe_2O_4$ with large specific surface area, J. Mater. Chem. 20 (2010) 945–952.
[28] Y.B. Wang, H.Y. Zhao, M.F. Li, J.Q. Fan, G.H. Zhao, Magnetic ordered mesoporous copper ferrite as a heterogeneous Fenton catalyst for the degradation of imidacloprid, Appl. Catal. B: Environ. 147 (2014) 534–545.
[29] W. Li, J. Liu, D.Y. Zhao, Mesoporous materials for energy conversion and storage devices, Nat. Rev. Mater. 1 (2016) 16023.
[30] Z.N. Liu, N.Q. Zhao, C.S. Shi, F. He, E.Z. Liu, C.N. He, Synthesis of three-dimensional carbon networks decorated with Fe_3O_4 nanoparticles as lightweight and broadband electromagnetic wave absorber, J. Alloy. Compd. 776 (2019) 691–701.
[31] Q.W. Chen, W. Zhong, J.N. Zhang, C.L. Gao, W.L. Liu, G.D. Li, M.M. Ren, Fe_3O_4 nanorods in N-doped carbon matrix with pseudo-capacitive behaviors as an excellent anode for subzero lithium-ion batteries, J. Alloy. Compd. 772 (2019) 557–564.
[32] X.J. Zhao, Y.H. Jia, Z.H. Liu, GO-graphene ink-derived hierarchical 3D-graphene architecture supported Fe_3O_4 nanodots as high-performance electrodes for lithium/sodium storage and supercapacitors, J. Colloid Interface Sci. 536 (2019) 463–573.
[33] A. Rumplecker, F. Kleitz, E.L. Salabas, F. Schüth, Hard templating pathways for the synthesis of nanostructured porous Co_3O_4, Chem. Mater. 19 (2007) 485–496.
[34] Y.J. Xu, W.Y. Bian, J. Wu, J.H. Tian, R.Z. Yang, Preparation and electrocatalytic activity of 3D hierarchical porous spinel $CoFe_2O_4$ hollow nanospheres as efficient catalyst for oxygen reduction reaction and oxygen evolution reaction, Eletrochim. Acta 151 (2015) 276–283.
[35] B.B. Anderson, S.E. Zerby, A.G. Ewing, Calculation of transmitter concentration in individual PC12 cell vesicles with electrochemical data and a distribution of vesicle size obtained by electron microscopy, J. Neurosci. Methods 88 (1999) 163–170.
[36] L. Wang, H.R. Xu, Y.L. Song, J.P. Luo, S.W. Xu, S. Zhang, J.T. Liu, X.X. Cai, Carbon fiber ultramicrodic electrode electrodeposited with over-oxidized polypyrrole for amperometric detection of vesicular exocytosis from pheochromocytoma cell, Sensors 15 (2015) 868–879.
[37] L. Amato, A. Heiskanen, C. Caviglia, F. Shah, K. Zór, M. Skolimowski, M. Madou, L. Gammelgaard, R. Hansen, E.G. Seiz, M. Ramos, T.R. Moreno, A. Martínez-Serrano, S.S. Keller, J. Emnéus, Pyrolysed 3D-carbon scaffolds induce spontaneous differentiation of human neural stem cells and facilitate real-time dopamine detection, Adv. Funct. Mater. 24 (2014) 7042–7052.
[38] H. Shinohara, Y. Sakai, T.A. Mir, Real-time monitoring of intracellular signal transduction in PC12 cells by two-dimensional surface plasmon resonance imager, Anal. Biochem. 441 (2013) 185–189.
[39] M.H. Akhtar, K.K. Hussain, N.G. Gurudatt, Y.B. Shim, Detection of Ca^{2+}-induced acetylcholine released from leukemic T-cells using an amperometric microfluidic sensor, Biosens. Bioelectron. 98 (2017) 364–370.
[40] H. Beitollahi, F.G. Nejad, S. Shakeri, GO/Fe_3O_4@SiO_2 core–shell nanocomposite-modified graphite screen-printed electrode for sensitive and selective electrochemical sensing of dopamine and uric acid, Anal. Methods 9 (2017) 5541–5549.
[41] W.W. Yang, Y.S. Yu, Y. Tang, K.Y. Li, Z. Zhao, M.G. Li, G.P. Yin, H.B. Li, S.H. Sun, Enhancing electrochemical detection of dopamine via dumbbell-like FePt-Fe_3O_4 nanoparticles, Nanoscale 9 (2017) 1022–1027.
[42] Y. Wang, Y. Zhang, C. Hou, M.Z. Liu, Ultrasensitive electrochemical sensing of dopamine using reduced graphene oxide sheets decorated with p-toluenesulfonate-doped polypyrrole/Fe_3O_4 nanospheres, Microchim. Acta 183 (2016) 1145–1152.
[43] J. Ghodsi, A. Hajian, A.A. Rafati, Y. Shoja, O. Yurchenko, G. Urban, Electrostatically immobilized hemoglobin on silica-coated magnetic nanoparticles for simultaneous determination of dopamine, uric acid, and folic acid, J. Electrochem. Soc. 163 (2016) B609–B616.